J Mater Sci (2008) 43:2625–2630
DOI 10.1007/s10853-008-2477-5

The effects of pre-implantation of steel substrates on the structural properties of TiN coatings

D. Peruško · M. Mitrić · V. Milinović · S. Petrović · M. Milosavljević

Received: 2 October 2007 / Accepted: 15 January 2008 / Published online: 20 February 2008

Abstract We have studied the effects of nitrogen pre-implantation of AISI C1045 steel substrates on the microstructure and microhardness of deposited TiN coatings. The substrates were implanted at 40 keV, to the fluences from 5×10^{16} to 5×10^{17} ions/cm^2, which was followed by deposition of 1.3-μm thick TiN coatings by reactive sputtering. Structural characterization of the samples was performed by standard and grazing incidence X-ray diffraction analysis, Rutherford backscattering spectroscopy and transmission electron microscopy. Microhardness was measured by the Vicker's method. Nitrogen implantation up to 2×10^{17} ions/cm^2 induces the formation of Fe_2N phase in the near surface region of the substrates, which becomes more pronounced for higher fluences. Microstructure of the deposited TiN coatings shows a strong dependence on ion beam pre-treatment of the substrates. The layers grown on non-implanted substrates have a (200) TiN preferential orientation, and those grown on implanted substrates have (111) TiN preferential orientation. The change in preferred orientation of the layers is assigned to a developed surface topography of the substrates induced by ion implantation, and possible effects of distorted and altered crystalline structure at the surface. Ion implantation and deposition of TiN coatings induce an increase of microhardness of this low performance steel for more than eight times.

D. Peruško (✉) · M. Mitrić · V. Milinović · S. Petrović · M. Milosavljević
VINČA Institute of Nuclear Sciences, P.O. Box 522, 11001 Belgrade, Serbia
e-mail: dperusko@vin.bg.ac.yu

Introduction

Surface treatment is becoming a crucial processing for improving the tribological properties of constructive and tool steel materials. Many techniques are now available for deposition of hard coatings, as well as ion beam processes such as ion implantation, plasma ion immersion, or ion beam assisted deposition. Modern surface treatments usually combine some of the layer deposition techniques and ion beam processing.

In the last decades there is an increasing interest in TiN coatings deposited by chemical or physical vapor deposition methods (CVD or PVD) [1]. Titanium-nitride is a refractory interstitial nitride with extreme hardness, corrosion resistance, and relatively high conductivity. The most successful application area of TiN coatings is for protection of various high speed tools. However, direct application of PVD hard coatings cannot guarantee optimal tribological performance without pre-treatment of the substrates. Many authors studied the beneficial effects of plasma nitriding of steel materials before PVD of hard coatings [2–5]. It is known that wear resistance strongly depends on the coating adhesion to the substrate, which was found to improve by pre-nitrating of tool steel materials.

Ion implantation was proven as a very powerful technique for improving tribological properties, both when applied directly on the processed materials or on previously deposited coatings [6, 7]. This arises from the non-equilibrium nature of the ion implantation process, enabling formation of metastable phases and structures unattainable by conventional treatments. It was shown that implantation of nitrogen ions into steel, stainless steel, and aluminum alloys leads to improvement of their mechanical and tribological properties [8–10].

In this work, we have studied the effects of nitrogen ion pre-implantation of AISI C1045 steel substrates on the properties of subsequently reactively sputtered TiN coatings. It was found that pre-implantation of the substrate influences both the microstructure of the coatings and their microhardness.

Experimental procedure

As a substrate material, we used AISI C1045 construction steel, cut in the form disks, 25 mm in diameter and 5 mm thick. Chemical composition of this material is shown in Table 1. The samples were mechanically prepared to a roughness parameter $R_a = 1.01$ μm.

Prior to the deposition of TiN coatings, the substrates were irradiated with N_2^+ ions in a 400 kV ion implanter. The ion energy was 40 keV per atom, which gives a projected range of 46 nm according to calculations by the TRIM code [11]. The ion beam was scanned homogenously over the substrate surface, at a beam current of 0.1 mA/cm^2. During implantation, the samples were cooled, so the temperature did not exceed 120 °C. The implanted fluences were in the range from 5×10^{16} to 5×10^{17} ions/cm^2.

The TiN coatings were deposited by reactive d.c. sputtering in a Balzers Sputtron II system. We sputtered a 99.9% pure Ti target with argon ions in nitrogen ambient. The deposition parameters were as follows: base pressure in the chamber 1.3×10^{-3} Pa, argon partial pressure 0.13 Pa, nitrogen partial pressure 4×10^{-2} Pa, the high voltage on the target −1.5 kV, the Ar^+ beam current 25 mA/cm^2, and the substrate temperature 200 °C. The TiN coatings were deposited to a thickness of 1.3 μm, at a rate of 0.12 nm/s. Before deposition of TiN, the substrates were cleaned by back sputtering, which was performed under the following conditions: Ar^+ energy was 1 keV, current density 8 μA/cm^2, and sputtering time 5 min. This removed about 3 nm of materials from the substrate surface. For transmission electron microscopy and Rutherford backscattering spectroscopy, we prepared 250 nm TiN films deposited under the same conditions on Si wafers. In the later case, we used a 10 nm intermediate Ti layer to improve adhesion.

Structural characterizations were performed by standard X-ray diffraction analysis (XRD), grazing incidence X-ray diffraction (GXRD), Rutherford backscattering spectroscopy (RBS), and transmission electron microscopy (TEM). For GXRD analysis, Cu K_α X-ray diffraction patterns were collected by Bruker D8 Advance Diffractometer with parallel beam optics. The incidence angle was 3°, the step 0.05° and the time interval 10 s per step. RBS analysis was done with a 900 keV He^{++} ion beam, at normal incidence, and a detector positioned at 165° backscattering angle. The experimental data were analyzed with the WiNDF code [12]. Cross-sectional TEM analysis was done on a Philips EM 400T microscope. Micro diffraction (MD) technique was used to study the crystalline structure of the samples. We also did micro-hardness measurements of the samples, by the Vicker's method, using a pyramidal indenter with the top angle of 136°.

Table 1 Chemical composition of AISI C1045 steel

Element	C	Mn	Si	P	S	Fe
at %	0.45	0.65	0.15–0.35	<0.045	<0.045	balance

Results and discussion

X-ray diffraction analysis was used to study the structure of as-implanted AISI C1045 substrates and of the deposited TiN coatings. However, since the range of implanted nitrogen was only a few tens of nm, standard XRD did not show any changes in the spectra taken from non-implanted and implanted substrates. Formation of Fe-nitride phases could only be detected by GXRD analysis. Though, standard XRD was sensitive enough to study the deposited 1.3-μm thick TiN coatings.

In Fig. 1a–d, we present an illustration of XRD and GXRD analyses of implanted substrates. A standard XRD spectrum taken from a sample implanted with nitrogen to 5×10^{17} ions/cm^2 is given in (a). It shows only a diffraction line that corresponds to Fe (110). In (b–d) we present the GXRD spectra. Here we observe only Fe diffraction peaks in the non-implanted sample (b) and the formation of Fe_2N phase in the implanted samples (c and d). It is seen that the Fe_2N phase is formed after implantation of nitrogen to 2×10^{17} ions/cm^2. Among the Fe_2N diffraction peaks, the most intensive is the one that corresponds to (211) orientation. After implantation to 5×10^{17} ions/cm^2 we only see a more pronounced nitriding effect and no appearance of new diffraction lines.

Calculations with the TRIM code gave a peak nitrogen concentration of 9.1×10^{22} at/cm^3, for the implanted fluence of 2×10^{17} ions/cm^2, and a sputtering yield of 0.89 atoms/ion. Concentration of Fe atoms in bulk iron is 8.4×10^{22} at/cm^3, and it is known that nitrogen has a fairly large diffusion coefficient in Fe at room temperature. However, despite the high sputtering yield and a high diffusivity, the GXRD analysis in our experiments shows that we have achieved the concentration of nitrogen necessary to form the Fe_2N phase. Kopcewicz et al. [13] have shown that implantation of nitrogen into bulk iron at a fluence of

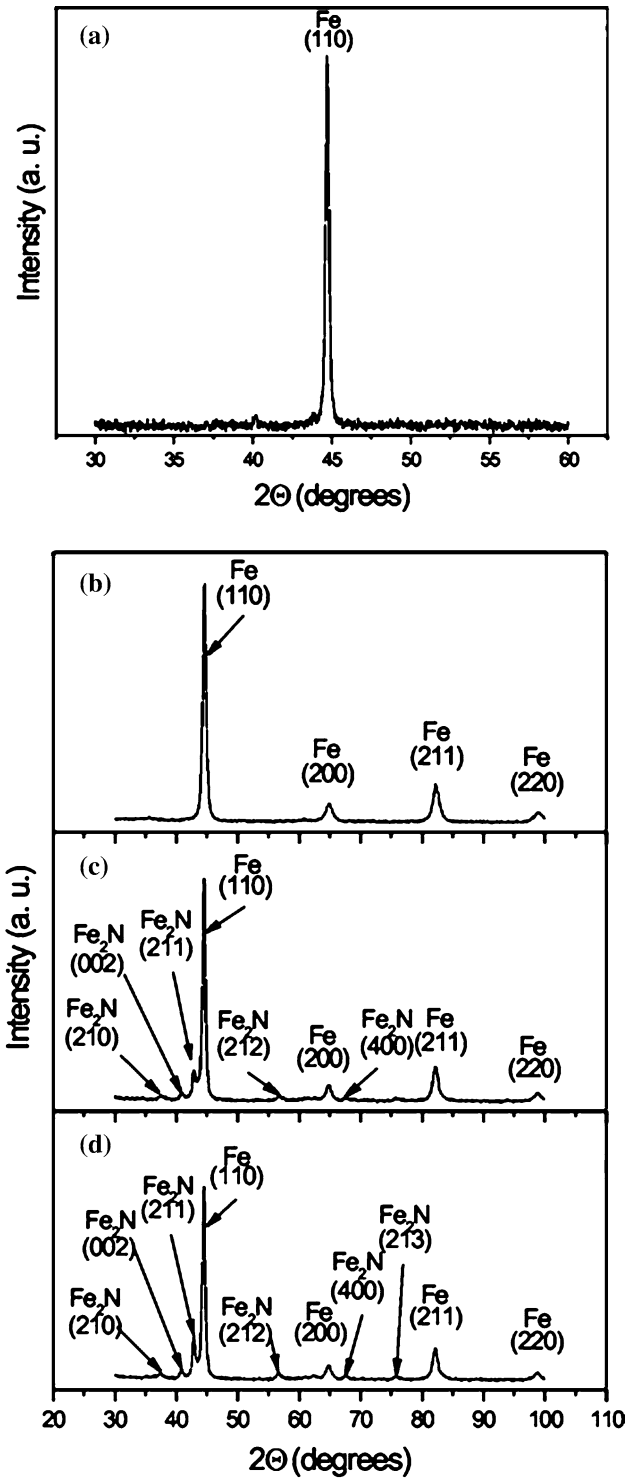

Fig. 1 XRD analysis of implanted steel substrates: (**a**) standard XRD spectrum from the sample implanted to 5×10^{17} ions/cm^2; GXRD spectra from samples: (**b**) non-implanted, (**c**) implanted to 2×10^{17} ions/cm^2, and (**d**) 5×10^{17} ions/cm^2

1.5×10^{17} ions/cm^2 induces formation of $Fe_{3-x}N$, while the formation of Fe_2N starts at 2×10^{17} ions/cm^2. Our results are in agreement with these findings.

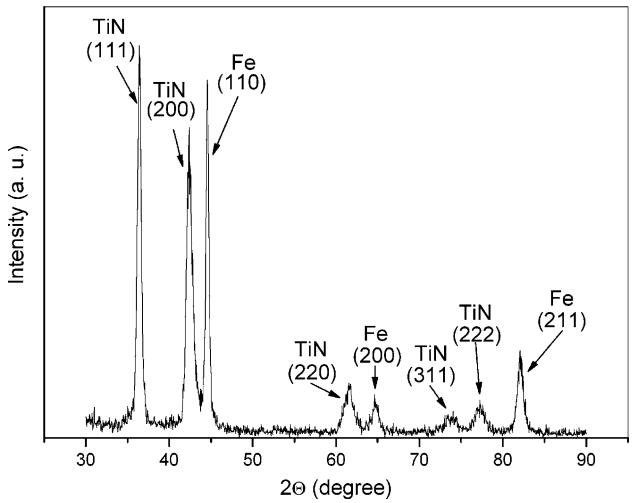

Fig. 2 Standard XRD spectrum from a substrate implanted with nitrogen to 5×10^{17} ions/cm^2 and covered by a 1.3 μm TiN coating

Figure 2 presents a standard XRD spectrum from an AISI C1045 substrate implanted with nitrogen to 5×10^{17} ions/cm^2 and covered by a 1.3 μm TiN coating. It shows the diffraction peaks that correspond to TiN and Fe. The Fe diffraction lines appeared from an uncovered part on the substrate surface. Usually, preferred orientation in TiN coatings deposited under similar conditions is either (111) or (200), depending on chemical composition of the substrate [14, 15]. In the case presented in Fig. 2, a clear preferred orientation does not exist.

GXRD analysis of (111) and (200) TiN diffraction peaks shows that the intensity ratio of these two lines depends on pre-implantation of the substrates. For illustration, in Fig. 3 we present GXRD spectra of a TiN film deposited on a non-implanted (a) and a layer deposited on a pre-implanted substrate to 5×10^{17} ions/cm^2 (b). It is necessary to mention that almost the same spectra were obtained by standard XRD analysis. The results of calculations made from these spectra are plotted in Fig. 4a, b. The ratio of the integrated intensities I(200)/I(111), is given in (a). The intensity of (200) TiN diffraction line is considerably higher in the coating deposited on non-implanted substrate. Pre-implantation of the substrate induces changes in the texture of the deposited coatings, the intensities of (200) and (111) diffraction lines becoming nearly the same. TiN is an anisotropic material, the XRD data base values give an intensity of (111) line as 75% of the (200) diffraction intensity [16]. This intensity ratio is marked as a dashed line in Fig. 4a. Our results indicate that on non-implanted substrates TiN layers grow with (200) preferential orientation. On the other hand, on all implanted substrates TiN layers have a (111) preferential orientation. This can be attributed to the changes in surface topography of the substrates induced by sputtering during ion implantation.

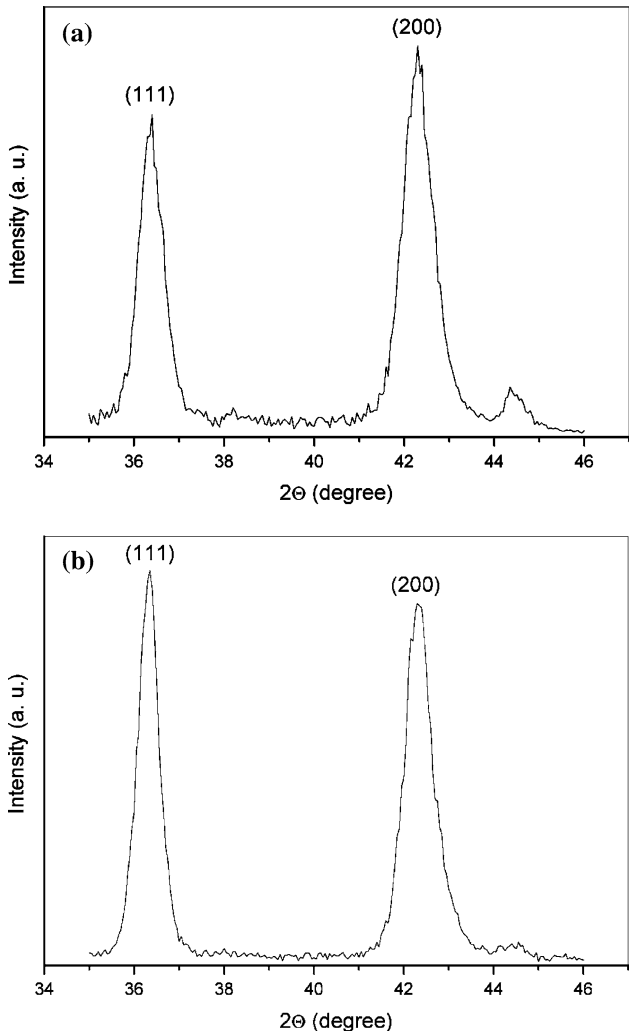

Fig. 3 GXRD spectra of (111) and (200) TiN diffraction peaks on non-implanted (**a**) and pre-implanted with ion fluence of 5×10^{17} ions/cm^2 (**b**) samples

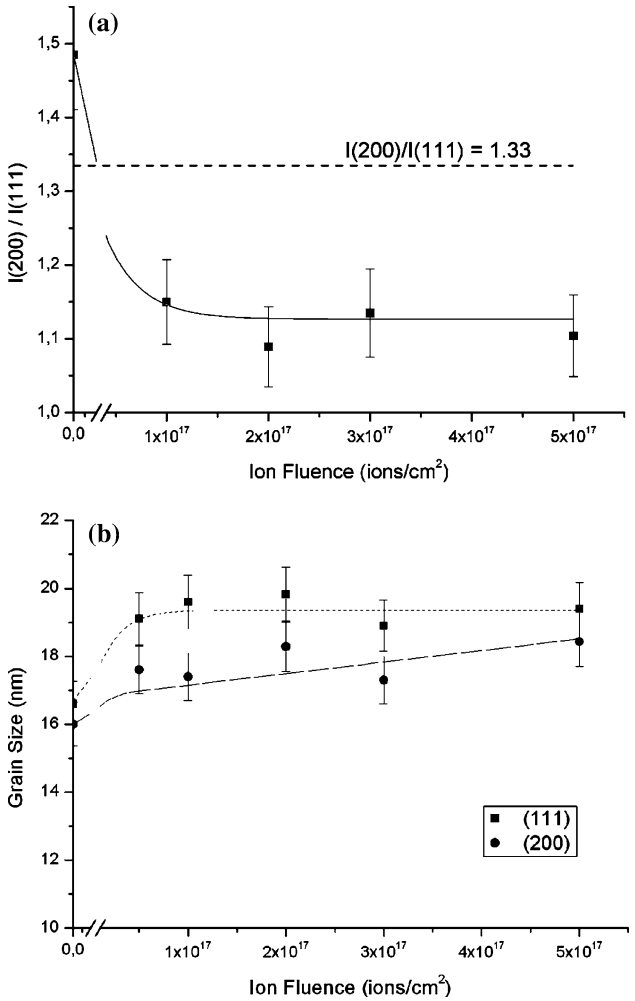

Fig. 4 Integrated intensity ratio I(200)/I(111) (**a**) and mean grain size (**b**) of TiN coatings as a function of ion fluence pre-implanted in the substrate

Taking the sputtering yield as 0.89 atoms/ion, implantation to 2×10^{17} ions/cm^2 sputters off approximately 20 nm of the substrate material.

Another effect of nitrogen pre-implantation of the substrates is the growth of TiN coatings with larger grains, as shown in Fig. 4b. To calculate the grain size, we used the corrected Scherrer equation [17]

$$D = \frac{a\,\lambda\,360 \cdot 10^{-10}}{2\,\pi\,\beta\,\cos\Theta}$$

where: a is the geometrical coefficient ($a = 0.9$ for cubic crystals), λ is the wavelength of the X-rays (for Cu K_α $\lambda = 1.5418 \times 10^{-10}$ m), $\beta = \sqrt{b^2 - B^2}$ is corrected line broadening, B is the FWHM of the peaks and b is a correction factor. The mean grain size increases from 16 to 16.5 nm for non-implanted substrates to 18–19 nm for substrates implanted to the highest fluence.

The change of I(200)/I(111) TiN diffraction intensity ratio described above can also be considered from another aspect. In Fig. 5, we have shown matching of the crystal lattices of iron and titanium nitride. In our case, the preferred orientation of Fe substrate lattice is (110), so the positions of Fe atoms are shown in that direction. On Fe lattice sites we have superimposed the Ti sites in (111) and (200) TiN lattice orientation. It is evident that better matching is achieved for (200) orientation of TiN, which may be the reason for this preferred orientation in the layers deposited on non-implanted substrates. Implantation to high fluences induces distortion of the substrate lattice in the near surface region, thus weakening the effect of Fe and TiN lattice matching. Pure iron has a body-centered cubic (bcc) crystal lattice. Formation of Fe_2N induces a transformation to the Fe_2N crystal lattice, which is distorted octahedral. Nitrogen atoms tend to locate at the octahedral interstitial sites. The type of chemical bonding in TiN is

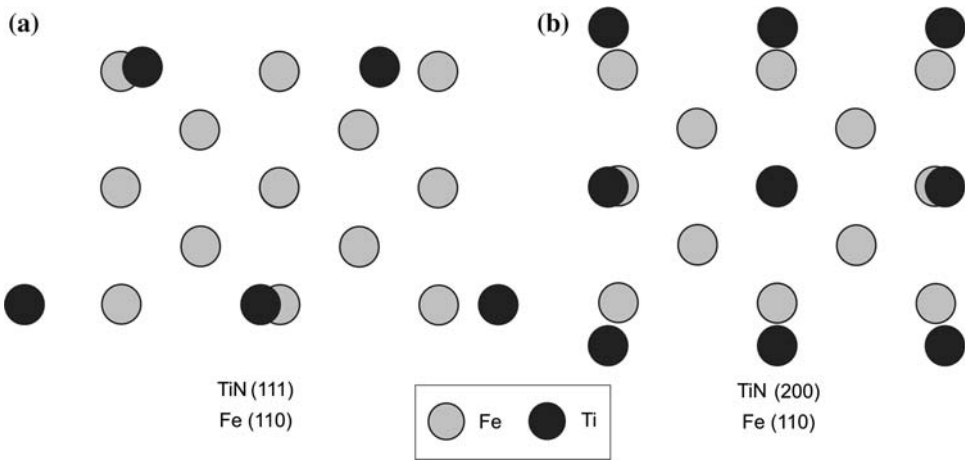

Fig. 5 Schematic view of crystal lattice matching of iron and titanium nitride

similar to that in Fe_2N, different compared to pure metallic bonding in bulk Fe. Our depositions were not done in ultra high vacuum, and hence we cannot claim an epitaxial relationship here. However, we did sputter cleaning of the substrates immediately before deposition, so there could be some influence on texturing and the growth of larger grains in TiN layers deposited on implanted substrates.

In Fig. 6, we present the results of cross-sectional TEM analysis. For this purpose, we deposited a 250 nm TiN film on a silicon wafer, under the same parameters as used for the steel substrates. The micrograph of a bright field image shows a polycrystalline columnar structure of the film. The columns stretch from the substrate to the surface, and their width is of the order of a few tens of nm. Comparing these results to those obtained by XRD analysis, there is a fair agreement in the column width. However, although individual columns may be longer, they can be twisted or disconnected in a thicker film. The electron diffraction pattern, taken with a focused micro-beam on the TiN layer, shows a polycrystalline structure. We observe individual spots lying on the rings that correspond to diffractions from (111) and (200) TiN planes, and from the planes with higher indexes.

Stoichiometry of the layers was analyzed by RBS. Again we have used a 250 nm TiN layer on Si wafer, because the depth resolution on a thicker layer would be poor. In Fig. 7a, b we have shown the experimental and fitted RBS spectra (a) and the extracted depth profiles of the components (b). In (a) we have also shown the separated spectra of the components obtained from the fit. It is seen that the

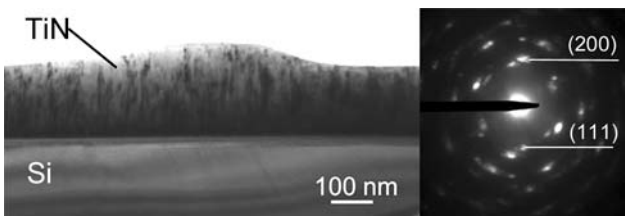

Fig. 6 Cross-sectional TEM analysis of a 250 nm TiN layer deposited on silicon

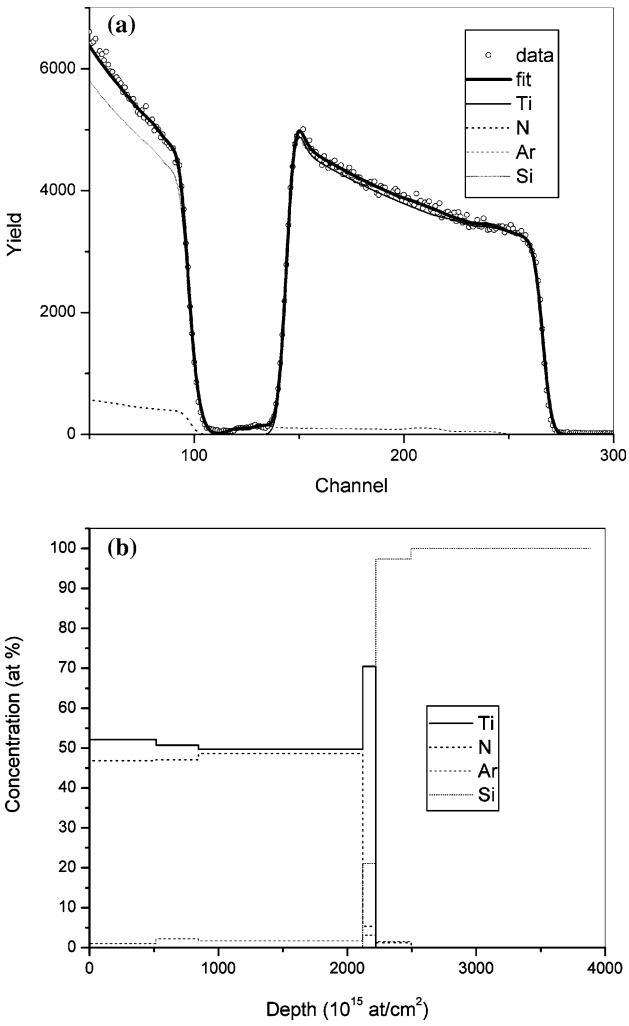

Fig. 7 Experimental and fitted RBS spectra (**a**) and the extracted depth profiles of the components (**b**) of a 250 nm TiN deposited on silicon

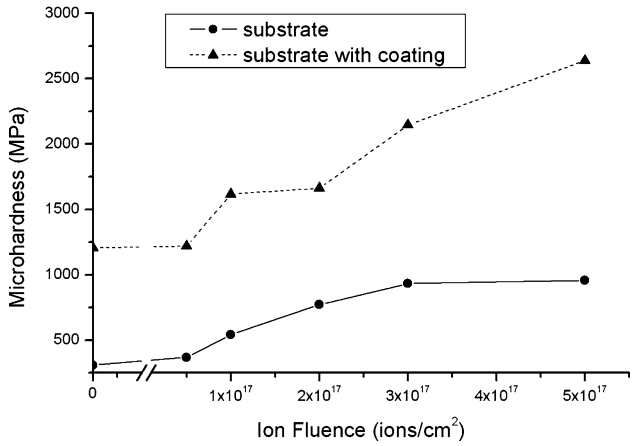

Fig. 8 The measured microhardness values before and after deposition of TiN coatings, as a function of pre-implantation fluence

Ti/N concentration ratio corresponds to stoichiometric TiN within 1–2 at%. A slightly higher Ti concentration near the Si substrate arises from a pure 10 nm Ti intermediate layer, which was deposited in order to improve the adhesion on Si. The layers contain 1–2 at% of Ar, which is incorporated during deposition. There is also a fraction of Ar at the substrate surface, because it was cleaned by back sputtering prior to deposition of the layers.

The results of micro-hardness measurements are shown in Fig. 8. Due to high value of surface roughness parameter R_a in this experiment we applied a load of 196 mN. The figure shows that ion implantation induces an increase of micro-hardness, both in as-implanted steel substrates and in the structures with deposited TiN coatings. The increased micro-hardness of the substrates can be associated with the enhanced formation of iron nitrides [15, 18] and radiation damage in the near surface region. This is further reflected on the deposited TiN coatings. It must be pointed out that for the applied load the indenter penetrates through the whole coating. The value of microhardness for coated sample irradiated to 5×10^{17} ions/cm^2 has more than eight times higher value than that for untreated sample. This illustrates the possibilities of these techniques (ion implantation and deposition of hard coatings) to improve the materials surface properties.

Conclusions

We have studied the effects of nitrogen pre-implantation of AISI C1045 construction steel substrates on the microstructure of sputter deposited TiN coatings. Implantation of 40 keV nitrogen induced the formation of Fe-nitrides, which is more pronounced for higher fluences. Microstructure of the deposited TiN coatings shows a strong dependence on ion beam pre-treatment of the substrates. They exhibit characteristic (200) and (111) TiN X-ray diffraction peaks, the ratio of their intensities depending on pre-implantation processing. The layers grown on non-implanted substrates have a (200) preferential orientation, and those grown on implanted substrates have (111) preferential orientation. These changes are assigned to a developed surface topography of the substrates induced by ion implantation, and possible effects of distorted and altered crystalline structure at the surface. Ion implantation and deposition of TiN coatings induce an increase of microhardness of this low performance steel for more than eight times.

Acknowledgements The authors gratefully acknowledge Prof H. Hofsaess for enabling RBS analysis at Goettingen University. This work was supported by the Ministry of Science and Environmental Protection of the Republic of Serbia (Project No. OI 141013) and partially by the International Atomic Energy Agency, Vienna.

References

1. Sundgren JE (1985) Thin Solid Films 128:21
2. Zeghni AE, Hashmi MSJ (2004) J Mat Proc Technol 155–156:1918
3. Sun Y, Bell T (1993) Wear 166:119
4. Van Stappen M, Kerkhofs M, Qaeyhaegens C, Stals L (1992) Wear 153:655
5. Hock K, Spies HJ, Larich B, Leonhardt G (1996) Surf Coat Technol 88:44
6. Canu E, Martinez L, Simancas J, Perez-Trujillo FJ, Gomez C, Bastidas JM (2006) Surf Coat Technol 200:5123
7. Sharkeev YP, Bull SJ, Perry AJ, Klingenberg ML, Fortuna SV, Michler M, Manory RR, Shulepov IA (2006) Surf Coat Technol 200:5915
8. Jones AM, Bull SJ (1996) Surf Coat Technol 83:269
9. Intarasiri S, Yu LD, Chudoba T, Reuther H, Ramelt U, Richter E (1998) Surf Coat Technol 99:305
10. Kukareko VA, Byeli AV (2000) Surf Coat Technol 127:174
11. Ziegler JF, Biersack JP, Littmark U (1985) The stopping and range of ions in Solids. Pergamon Press, New York
12. Barradas NP, Jeynes C, Webb RP (1997) Appl Phys Lett 71:291
13. Kopcewicz M, Jagielski J, Matz W (2002) Hyperfine Interact 139/140:369
14. Škorić B, Kakaš D, Rakita M, Bibić N, Peruško D (2004) Vacuum 76:169
15. Peruško D, Popović M, Novaković M, Bibić N (2005) In: Popović Z, Maričić AM (eds) Proceedings of VI Scientific Meeting: Physics and Technology of Materials, Čačak, Serbia, August 2005. Technical Faculty of Čačak p 31
16. Wong-Ng W, Mcmurdie H, Paretzkin B, Hubbard C, Dragoo A (1987) NBS, Gaithersburg, MD, USA, ICDD Grant-in-Aid
17. Klung HP, Alexander LE (1974) In: X-ray diffraction procedures, Chap. 7. J. Willey & Sons
18. Youssef AA, Budzynski P, Feliks J, Kobzev AP, Sielanko J (2004) Vacuum 77:37